IJST, Transactions of Civil and Environmental Engineering, Vol. 35, No. C1, pp 81-94
Printed in The Islamic Republic of Iran, 2011


# STEADY-STATE DEFORMATION BEHAVIOUR OF ASPHALTIC MIXTURES*

H. TAHERKHANI AND M. JAVANMARD**

Dept. of Civil Engineering, University of Zanjan, I. R. of Iran
Email: mehranjav@yahoo.com

**Abstract–** Permanent deformation of asphaltic materials has a major contribution to rutting. Under static loading, the steady-state deformation of asphaltic materials is the key component of the permanent deformation. The steady-state deformation behaviour of a standard 70/100 penetration grade pure bitumen and two types of asphaltic mixtures used in the UK pavements, namely a 10mm Dense Bitumen Macadam (DBM), which is a dense graded mixture, and a 30/10 Hot Rolled Asphalt (HRA), which is a gap graded mixture have been studied. Using Dynamic Shear Rheometer (DSR) Constant stress creep tests were conducted on the bitumen at 10°C and 20°C over a range of stress levels. Uniaxial creep and constant strain rate tests have been conducted over a range of stress levels, strain rates and temperatures, and triaxial creep tests have been conducted over a range of stress levels and confining pressures on the mixtures. The steady-state deformation behaviour of the bitumen is found to be linear at stress levels less than 100 kPa and non-linear power law creep with a power exponent of 2.6 at stress levels higher than 500 kPa. The steady-state deformation behaviour of both mixtures is found to be well captured by the Modified Cross Model which predicts linear viscous behaviour at low stress levels and non-linear viscous behaviour at high stress levels. The steady-state deformation behaviour of the DBM mixture is found to be more sensitive to the stress level. The temperature dependency of the steady-state deformation behaviour is found to be well captured by the Williams-Landel-Ferry (WLF) equation. It is found that confinement has a stiffening effect on the steady-state deformation behaviour of the mixtures. The stiffening effect of the confining stress is found to be higher for the DBM mixture.

**Keywords–** Bitumen, creep, uniaxial, triaxial, steady-state, deformation

## 1. INTRODUCTION

Pavement materials fail under the loading and environmental conditions over the life of highways. Development of constitutive models for describing the failures has been the challenge of researchers [1]. Rutting (permanent deformation) of asphalt pavements is one of the most common forms of road failure. Permanent deformation of bituminous layers contributes significantly to the rutting and is due to a combination of densification and shear deformation. For bituminous mixtures that are well compacted during construction, it has been found that the shear deformation is the primary cause of rutting [2-4]. Shear deformation of bituminous mixtures is due to the viscous behaviour of the mix and usually manifests itself as ridges adjacent to the wheel path. When a wheel load is applied on an element of bituminous material in a pavement, it causes some deformation in the material. After passing the load, part of the deformation recovers, and some remains in the material as permanent deformation. Accumulation of these permanent deformations results in pavement rutting.

Over the last decade, the quasi-static deformation behaviour of pure bitumen and idealised asphaltic mixtures has been studied at the Universities of Cambridge and Nottingham. Using the results of uniaxial

*Received by the editors July 25, 2009; Accepted June 21, 2010.
**Corresponding author

tension and compression and shear tests, Cheung *et al.* [5 and 6] investigated the quasi-static mechanical properties of a standard 50 penetration grade bitumen over a wide range of stress conditions, strain rates, temperatures and pressures. A deformation mechanism map was constructed and divided into various regions, each described by a physical model. Based on experimental results, Cheung *et al.* [5] found that, at temperatures above the glass transition, the steady-state deformation behaviour of the 50 penetration grade bitumen was linear viscous at low stress levels, and non-linear power law creep at high stress levels with a creep exponent of approximately 2.3. The transition from linear to nonlinear behaviour was found to occur at a stress level of 115 kPa. Using the Dynamic Shear Rheometer, Collop *et al.* [7] proposed a model for describing the deformation behaviour of the bitumen subjected to shear loading in the DSR. The model assumed linear behaviour at low stress levels (<50 kPa), power law creep behaviour at high stress levels (>100 kPa), and a transition region from linear to nonlinear behaviour for stress levels between 50 and 100 kPa. The monotonic uniaxial and triaxial steady-state deformation behaviour of idealised bituminous mixtures (sand asphalts) was investigated by Deshpande *et al.* [8], Collop *et al.* [9] and Ossa [10]. They found that the steady-state deformation behaviour of the dense graded idealised mixtures (more than 64% volume fraction of aggregate) was strongly dependant on the confining stress. For a constant stress ratio, defined as the mean stress divided by the deviator stress, the steady-state axial creep behaviour was found to have the same form as pure bitumen with linear viscous behaviour at low stress levels and non-linear viscous behaviour at higher stress levels.

This paper describes the steady-state viscous deformation of two types of realistic asphaltic mixtures commonly used in UK flexible pavements.

## 2. MATERIALS

Two generic types of asphaltic mixture were chosen for this study; a 10mm Dense Bitumen Macadam (DBM) [11] and a 30/10 Hot Rolled Asphalt (HRA) [12]. These mixtures were chosen because different types of behaviour were anticipated for them. The DBM is a continuously graded mixture that relies primarily on aggregate interlock for its strength, whereas the HRA is a gap graded mixture that relies more on the properties of the bitumen/sand/filler mortar. To study the effect of different aggregate structures on the deformation behaviour of the mixtures, without the influence of different bitumen types, the same 70/100 penetration grade bitumen was used in both mixtures. The measured Ring and Ball softening point and Penetration value of the bitumen were 45°C and 88 dmm Pen respectively. The design aggregate grading for the DBM and HRA are shown in Figs. 1 and 2, respectively. The figures also show the grading limits recommended in BS: 4987, Part 1 [11] and BS: 594, Part 1 [12] for the 10 mm DBM and HRA 30/10, respectively.

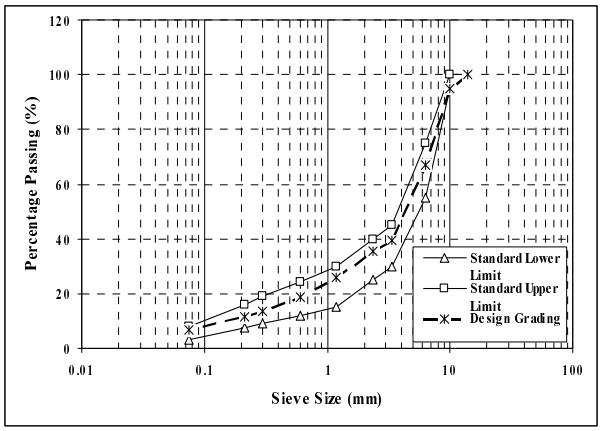


Fig. 1. Aggregate gradations of 10mm DBM

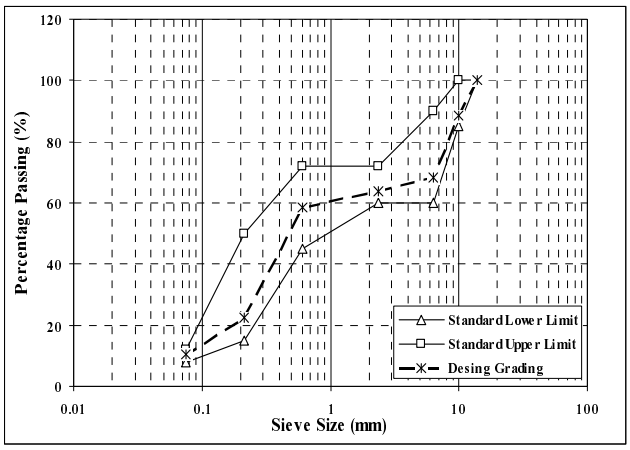


Fig. 2. Aggregate gradation of the HRA30/10

The objective of this research was to study the deformation behaviour of realistic asphaltic mixtures after initial compaction by traffic. Therefore, the target air void content for both mixtures was set at 4%. The binder contents of 5.5% and 8% were chosen for the DBM and HRA respectively.

An ideal specimen for this research would be a specimen with a uniform air void distribution and an aggregate orientation similar to that found in the real pavement. Homogeneity of a mixture is controlled by the compaction effort, method of compaction, viscosity of bitumen, aggregate gradation and aggregate shape. Specimens cored from slabs compacted by a roller compactor were shown to be nonuniform and not suitable for creep testing [13].

A gyratory compactor was used for manufacturing the specimens for this study. Gyratory compaction attempts to reproduce field compaction of hot asphalt mixtures by applying a vertical compressive stress and a gyratory action at the same time. The gyratory action generates horizontal shear stresses in the mixture as applied by the moving road rollers. The principle of gyratory compaction is to rotate a mould on an axis eccentric to the vertical and apply a fixed pressure to the material inside the mould through parallel end plates. The 150mm diameter moulds were used for gyratory compaction, and cylindrical specimens, 100mm in diameter and 100mm in height cored from gyratory compacted mixtures were manufactured for the testing programme, as shown in Fig. 3.

Fig. 3. Test Specimen

Measurements of density and air void content were undertaken in accordance with BS 598 [14] and only specimens with an air void content between 3% and 5% were selected for testing. The specimens were stored in a cold room at 5˚C until they were required for testing.

## 3. STEADY-STATE DEFORMATION BEHAVIOUR OF BITUMEN

### *a) Dynamic Shear Rheometer*

Dynamic shear Rheometers (DSRs) are used to measure rheological characteristics of bitumen, such as complex modulus and phase angle from which elastic and viscous properties can be defined [15]. Fig. 4

shows the principles involved in the DSR test. In the DSR test, the bitumen is sandwiched between a spindle and a base plate. The spindle, which can be either disc-shaped or conical, is allowed to rotate while the base plate remains fixed during testing. The DSR test can be carried out in controlled stress or controlled strain mode. In the controlled stress mode, a specified magnitude of shear stress at half the radius of disc (R/2) is applied to the bitumen by application of a torque to the spindle.

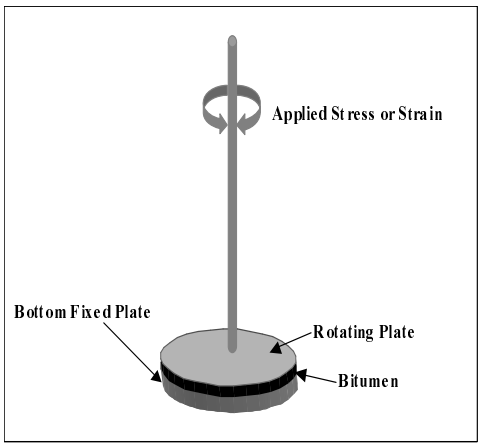


Fig. 4. Principle of torsinal-type dynamic shear Rheometer (DSR)

The resultant spindle rotation is measured, from which the magnitude of the shear strain is calculated at the edge of the disc (R). In the controlled strain mode, the magnitude of spindle rotation (i.e., magnitude of shear strain at the edge of the disc) is specified and the required torque needed is measured.

### *b) Apparatus*

DSR test set-up (Fig. 5) consists of parallel metal plates, a temperature control chamber, a loading device and a control and data acquisition system. The metal plates are typically 8 or 25 mm in diameter with smooth polished surfaces. A temperature control water chamber regulates the temperature of the specimen. Water is pumped through the test chamber by a separate circulating bath temperature control unit. The temperature control chamber and the circulating bath unit control the temperature of the specimen to an accuracy of ±0.1°C [11]. The temperature control chamber completely encloses the specimen between the top and bottom plates to minimise thermal gradients. When the test is stress controlled, the loading device applies a torque to an accuracy within 10 mN.m of the specified torque.

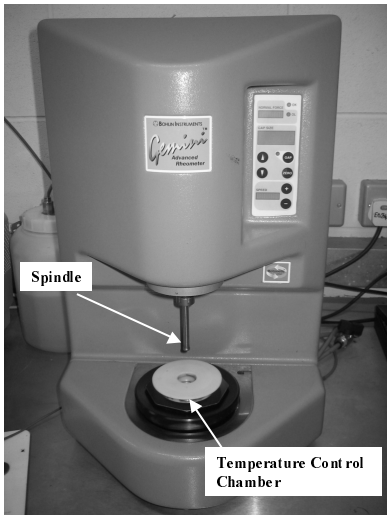


Fig. 5. Dynamic shear Rheometers (DSRs)

When the test is strain controlled, the loading device applies a torque sufficient to cause an angular rotational strain accurate within 100 μradians of the specified strain. The test data (temperature, angular rotation and torque) are recorded by the control and data acquisition system.

### *c) Test specimen preparation and test procedure*

The bitumen is heated, stirred occasionally (to ensure homogeneity and remove air bubbles) and then poured into small containers to be used for testing when required. To use the bitumen for testing, the container of bitumen is placed in an oven set at 140°C for about 15 minutes to ensure that it is fluid enough. By setting the temperature of the environmental water chamber, the lower and upper plates are heated to a temperature of approximately 50°C. Then, after raising the upper plate and drying the surfaces of the upper and lower plates, a sufficient amount of heated bitumen from the container is poured onto the centre of the bottom fixed plate. The loading mechanism along with the upper plate is then lowered to the required gap plus 50 μm. The excess bitumen, squeezed out between the lower and upper plates, is trimmed from the specimen by moving a heated trimming tool around the upper and lower plate perimeters. When the trimming is completed, the gap between the lower and upper plates is decreased by 50 μm to the desired testing gap (2000 μm). The cover of the environmental water chamber is then replaced, ensuring that both the upper and lower plates and the bitumen specimen are immersed in water. The temperature of the environmental water chamber is set to the test temperature, and once the desired test temperature is achieved, it remains at that temperature for at least 10 minutes [15], to ensure uniform test temperature in the bitumen specimen. Then the test is started.

The shear creep tests, in which the desired shear stress is applied to the specimen and held constant for a specified time, are performed on the pure bitumen over a range of stress levels from 400 Pa to 1000 kPa, at 10°C and 20°C. In these tests, a shear stress $\tau$ is applied rapidly to the specimen and then held constant. The material is allowed to creep until failure.

### *d) Test results*

A typical monotonic shear creep test result on the 70/100 penetration grade of bitumen at 20°C is shown in Fig. 6, where the creep shear strain at the outside of the disc is plotted against the time elapsed after the application of the stress.

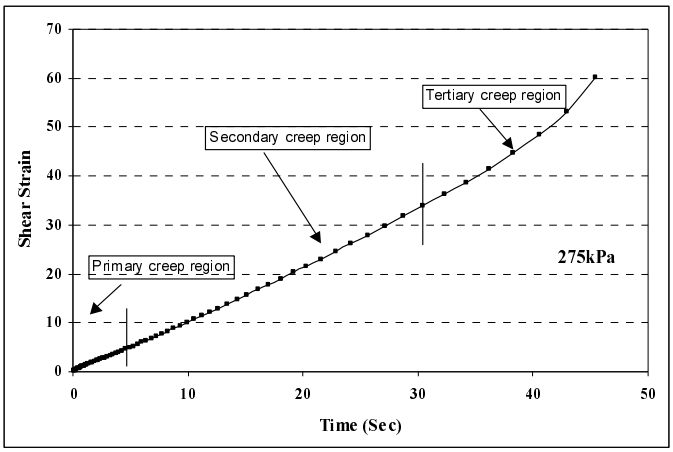


Fig. 6. Typical creep test results for the 70/100 Pen grade bitumen

The shear strain, shear strain rate and shear stress are calculated at the outside of the disc-shaped plates using:

$$\gamma_d = \frac{\theta R}{h} \qquad \dot{\gamma}_d = \frac{\theta \dot{R}}{h} \quad , \qquad \text{and} \qquad \tau_d = \frac{2T}{\pi R^3} \tag{1}$$

Where $\gamma_d$, $\dot{\gamma}_d$ and $\tau_d$ are the DSR shear strain, shear strain rate and shear stress, respectively. $T$ is defined as the torque, $R$ is the radius of parallel disks, $\theta$ and $\dot{\theta}$ are the angular rotation and the angular velocity and $h$ is the gap between the lower and upper plates (2 mm in these tests). As can be seen in Fig. 6, the creep curve can be divided into three regions: a primary creep region where the strain rate decreases, a secondary creep region where the strain rate is approximately constant and a tertiary creep region where the strain rate increases. The slope of the secondary creep region, in which the strain varies linearly with time, is defined as the steady-state strain rate at the prescribed stress, in line with the prescription of Cheung *et al.* [5], Collop *et al.* [7] and Ossa *et al.* [16].

Figure 7 summarises the monotonic steady-state behaviour of the bitumen over a range of stress levels at 10°C and 20°C, where the shear strain rate is plotted against the steady-state creep shear stress on a log-log scale. It can be seen that the steady-state deformation behaviour of the binder at both temperatures is similar in shape, with higher strain rates at 20°C for a particular stress level. It can also be seen that at low stress levels (<approximately 100 kPa) the experimental data points tend to lie on a straight line with a slope of approximately 1. This indicates that the steady-state deformation behaviour of the bitumen in this region is linear viscous ($\dot{\gamma} \propto \tau$). At stress levels greater than 100 kPa the slope of the line tends to increase, indicating a transition from linear viscous behaviour to non-linear viscous behaviour.

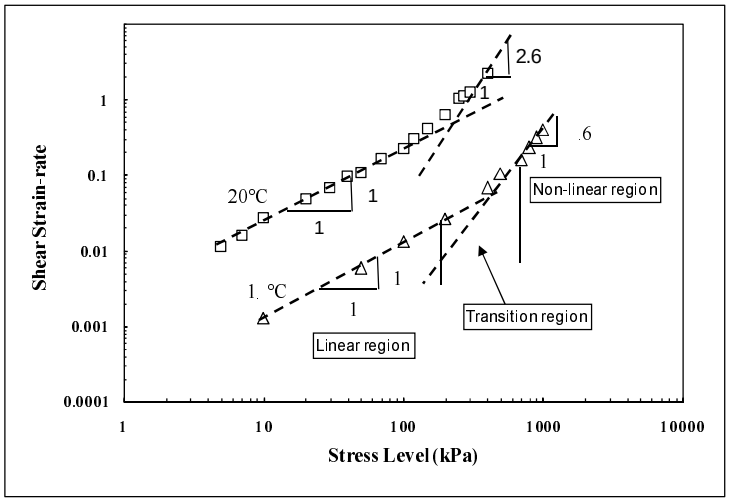


Fig. 7. Steady-state deformation behaviour of the 70/100 Pen grade bitumen

At stress levels greater than 500 kPa, the experimental data points tend to lie on a straight line again with a slope of 2.6, indicating non-linear power law creep viscous behaviour ($\dot{\gamma} \propto \tau^{2.6}$). The linear and non-linear behaviour of the binder can also be seen in Fig. 8 where the shear viscosity of the binder ($\eta = \tau / \dot{\gamma}$) is plotted against the shear stress. At low stress levels, the viscosity is constant, indicating linear behaviour and tends to decrease as the stress level increases, which indicates that the behaviour is non-linear at high stress levels.

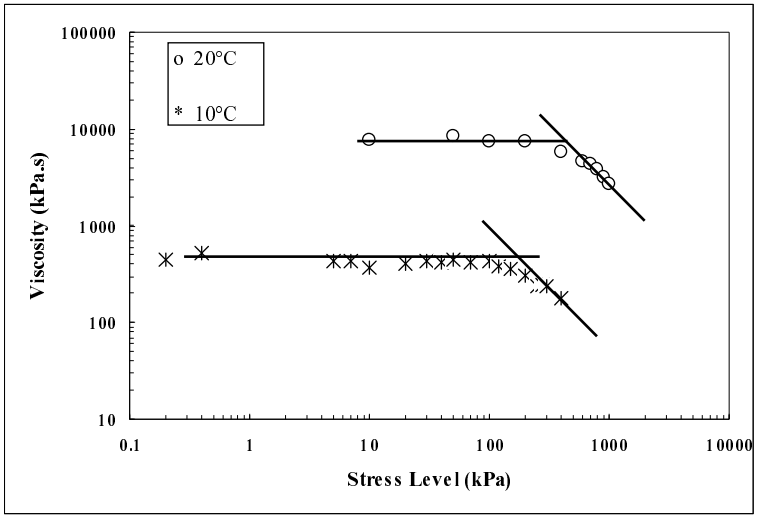


Fig. 8. Linear and non-linear behaviour of the 70/100 Pen grade bitumen

## 4. STEADY-STATE DEFORMATION BEHAVIOUR OF ASPHALTIC MIXTURES

### *a) Testing program*

Uniaxial tests were conducted over a range of stress levels, strain rates and temperatures. Table 1 and 2 show the uniaxial constant stress and constant strain rate tests program, respectively.

Table 1. Uniaxial constant stress creep test conditions

| Temperature (˚C) | Stress Level (kPa) | |
|---|---|---|
| | HRA30/10 | 10mm DBM |
| 10 | 1500, 2000 | 2000, 2500 |
| 20 | 60, 100, 1000, 1500, 2000 | 1000, 1500, 2000 |
| 40 | 400, 500 | 300, 500, 750 |

Table 2. Uniaxial constant strain rate test conditions

| Temperature (˚C) | Strain Rate (1/s) | |
|---|---|---|
| | HRA30/10 | 10mm DBM |
| 10 | 0.00005, 0.0005, 0.005 | 0.00005, 0.0005, 0.005 |
| 20 | 0.00005, 0.0005, 0.005 | 0.00005, 0.0005, 0.005 |
| 40 | 0.00005, 0.0005, 0.005 | 0.00005, 0.0005, 0.005 |

The triaxial tests were performed at 35˚C to avoid problems associated with handling the specimens at higher temperatures, as the softening point of the binder was 46˚C. The tests were performed over a range of confining and deviator stresses as given in Table 3. The stress conditions were characterised by the stress ratio $\eta = \sigma_m / \sigma$ **,** defined by Deshpande [17].

Table 3. Triaxial test conditions

| Mixture | Stress Ratio | Deviator Stress (kPa) |
|---|---|---|
| HRA30/10 | 0.33, 0.56, 0.70 | 300, 500, 700 |
| 10mm DBM | 0.33, 0.46, 0.56 | 500, 750, 1000 |

The mean stress ( $\sigma_m$ ), and the deviator stress ( $\sigma$ ) acting on the specimen are given by:

$$\sigma_m = \frac{\sigma_{33} + \sigma_{22} + \sigma_{11}}{3} \tag{2}$$

$$\sigma = \sigma_{33} - \sigma_{11} \tag{3}$$

where $\sigma_{11}$, $\sigma_{22}$ and $\sigma_{33}$ are the principal stresses. The HRA was tested up to a maximum stress ratio of $\eta$=0.7, whereas the DBM was only tested up to a maximum stress ratio of 0.56. This was because stress ratios above these values resulted in specimen lock-up and gave no meaningful results.

***b) Test equipment and instrumentation***

An Instron 1332 load frame with a temperature-controlled cabinet (–5˚C to 50˚C) and a servo-hydraulic actuator with a load capacity of ±100 kN and ±50mm axial stroke was used for the triaxial test programme. Figure 9 shows the experimental set-up for the compressive uniaxial testing undertaken in this study.

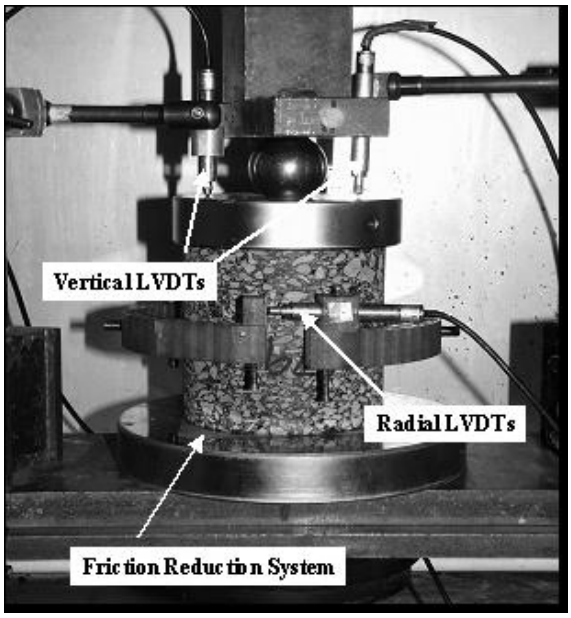


Fig. 9. Uniaxial test set-up

In this test, the specimen was placed between two polished chrome plates. A friction reduction system, comprised of a layer of plastic film sandwiched between two layers of soap, was used to minimize lateral confinement due to friction between the platens and the specimen. Two LVDTs, positioned on the top platen were used to measure the axial deformation of the specimen and an LVDT mounted on the collar was used to measure radial deformation at the mid-height of the specimen.

The triaxial test equipment, as illustrated schematically in Fig. 10, was comprised of three main parts, the servo-control hydraulic machine as described above, a triaxial cell placed in the temperature-controlled cabinet, and an air compressor to apply the confining pressure. The cell was a standard type commonly used in soil mechanics with a maximum confining pressure of 1.7 MPa. An impervious latex membrane was used to seal the specimens from the air inside the cell, which was used as the confining medium. The axial deformation of the specimen was measured using the load line displacement of the actuator. Similar to the uniaxial tests, the radial deformation was measured using an LVDT mounted on the collar through a sealed hole in the membrane.

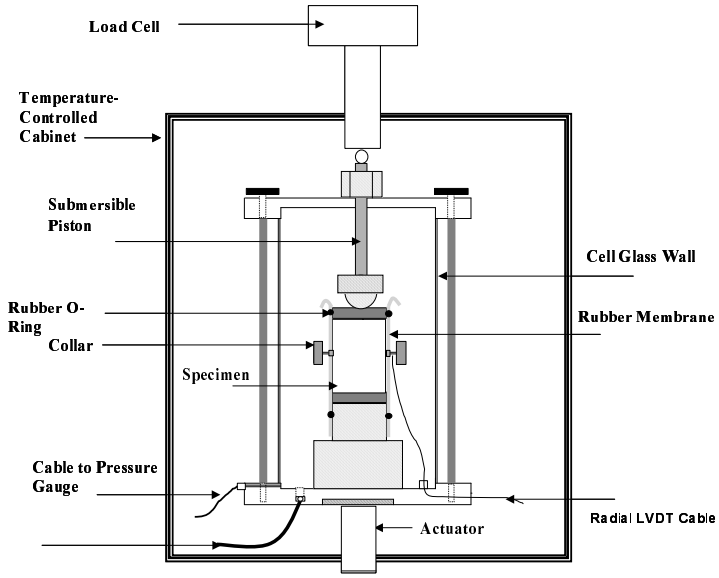


Fig. 10. Schematic of the triaxial cell

### *c) Test procedure*

**1. Uniaxial tests:** Uniaxial constant strain rate and constant stress creep tests were performed over a range of temperatures (10°C to 40°C). To ensure uniformity of temperature, the specimens were stored in a temperature-controlled cabinet for at least 12 hours prior to testing. The specimen was instrumented and a small compressive pre-load was applied to take up any slack in the system and allow the friction reduction system to deform in order to minimise subsequent measurement errors. A constant load or displacement rate was then applied to the specimen until failure. Axial and radial deformations and load measurements at pre-set time intervals were logged automatically during the test.

**2. Triaxial tests:** The target confining pressure was applied to the specimen followed by the preload stress, which was immediately followed by the target axial stress. The axial and radial deformations were automatically logged by the computer for the duration of the test. Only creep testing was undertaken in the triaxial testing programme.

In the triaxial tests, because of the axial symmetry, two of the principle stresses are equal to the confining stress. The third principal stress is equal to the sum of the confining stress and an additional axial stress which is applied. Hence, the principal stresses are given by:

$$\sigma_{33} = \frac{Q}{A} + p$$
$$\sigma_{22} = \sigma_{11} = p \tag{4}$$

Where Q is the applied axial load, $A$ is the initial cross-sectional area of the specimen and $p$ is the confining stress.

### *d) Test results*

**1. Uniaxial test results:** Typical uniaxial creep test results for the 10 mm DBM at selected testing conditions are presented in Fig. 11, where the axial strain is plotted against time. It can be seen from this figure that the creep curve can be divided into three regions: a primary creep region where the strain rate decreases, a secondary creep region where the strain rate is almost constant, known as the steady-state strain rate, and a tertiary creep region where the strain rate increases rapidly.

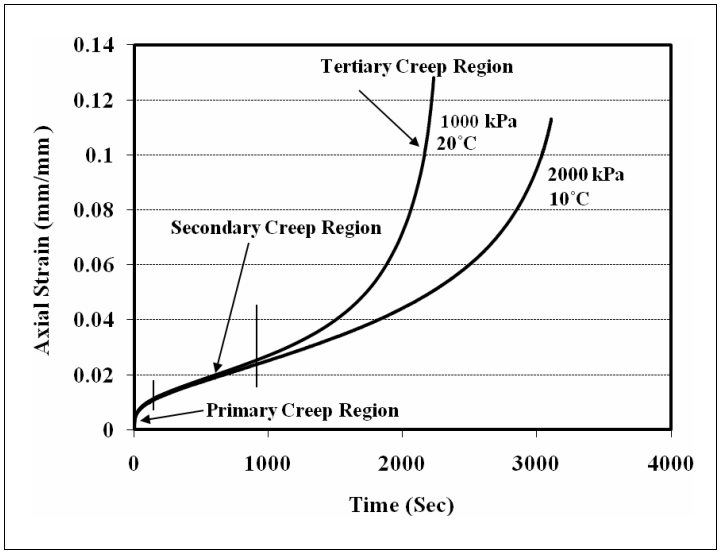


Fig. 11. Typical uniaxial creep test results for the 10 mm DBM

Figure 12 shows typical results from constant strain rate tests on the 10 mm DBM at selected test conditions, where axial stress is plotted against the axial strain. It can be seen from this figure that there is an increase in the steady-state stress with an increasing strain rate and/or decreasing temperature. It was found that the steady-state stress values for the DBM were greater than those for the HRA30/10.

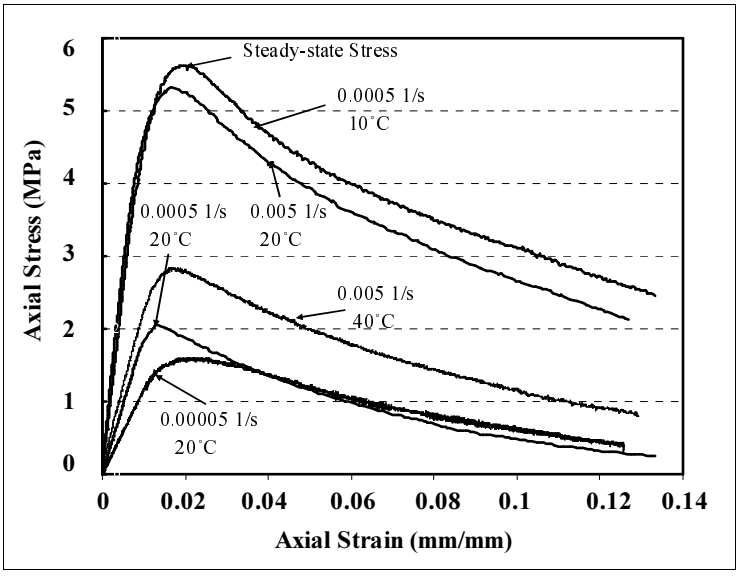


Fig. 12. Typical constant strain rate test results for the 10 mm DBM

The steady-state results from the constant stress creep and constant strain rate tests for the HRA are summarised in Fig. 13, where the steady-state strain rate is plotted against the steady-state stress on log-log scales. Similar behaviour was observed for the DBM which, for brevity, is not presented here. The steady-state stress in the constant strain rate tests is the peak stress at the prescribed strain rate and the steady-state strain rate in constant stress creep tests is the slope of the secondary creep region. It has previously been found that results from creep tests and constant strain rate tests are complementary [18, 10 and 19].

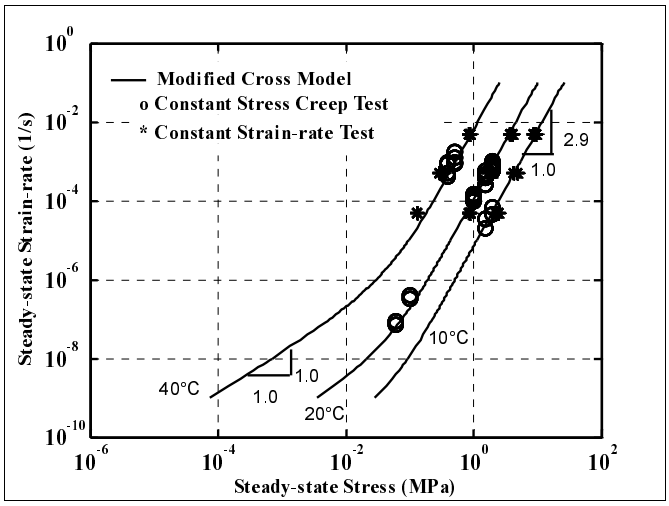


Fig. 13. Uniaxial steady-state deformation behaviour for the HRA30/10

Cheung [18] and Deshpande [17] proposed the Modified Cross Model to relate the steady-state stress to the steady-state strain rate:

$$\sigma = \frac{\sigma_0 \dot{\varepsilon}}{\dot{\varepsilon}_p}\left\{1 + \left(\frac{\dot{\varepsilon}}{\dot{\varepsilon}}\right)^m\right\}^{-1} \tag{5}$$

where $\sigma$ is the uniaxial stress, $\dot{\varepsilon}$ is the uniaxial strain-rate and $\sigma_0, m, \dot{\varepsilon}_p$ are the material constants. It can be seen that for low values of $\dot{\varepsilon}$, Eq. (5) reduces to linear viscous behaviour ($\dot{\varepsilon} \propto \sigma$) and for high values of $\dot{\varepsilon}$, Eq. (5) reduces to non-linear viscous behaviour ($\dot{\varepsilon} \propto \sigma^n$), where the exponent *n* is given by $1/(1-m)$. The solid lines in Fig. 13 are predictions from the Modified Cross Model.

For the three temperatures investigated in this study, the temperature dependence of the HRA and DBM mixtures was found to be well captured by the free volume WLF model which can be incorporated into Eq. (5) through the constant $\dot{\varepsilon}_p$ ( see Cheung [18] for further details) giving:

$$\dot{\varepsilon}_p = \dot{\varepsilon}_{pc} \exp\left(\frac{2.303 c_1^s (T - T_s)}{c_2^s + (T - T_s)}\right) \tag{6}$$

where $\dot{\varepsilon}_{pc}$ is the reference strain rate at T=0°C, $c_1^s$ & $c_2^s$ = universal constants with the values 8.86 & 101.6, and $T_s$ is the reference temperature with a value of 30°C. Equations (5) and (6) were fitted to the data; the constants are given in Table 4.

Table 4. Modified Cross Model constants for the mixtures

| Parameter | HRA | DBM |
|---|---|---|
| $\sigma_0$ (MPa) | 0.041 | 0.1 |
| $\dot{\varepsilon}$ (1/s) | $8.7\times10^{-8}$ | $8.7\times10^{-9}$ |
| *M* | 0.66 | 0.75 |

**2. Triaxial tests results:** Figure 14 summarises the monotonic triaxial steady-state creep behaviour of the HRA over a range of deviator stresses $\sigma$ and stress ratios $\eta$, where the steady-state strain rate $\dot{\varepsilon}$ is plotted against stress $\sigma$ on double logarithmic scales. Similar behaviour was observed for the DBM,

which for brevity, is not presented here. It can be seen from Fig. 14 that, for a constant stress ratio, the curves have the same shape as the curve for uniaxial behaviour ($\eta$=1/3) shown in Fig. 13.

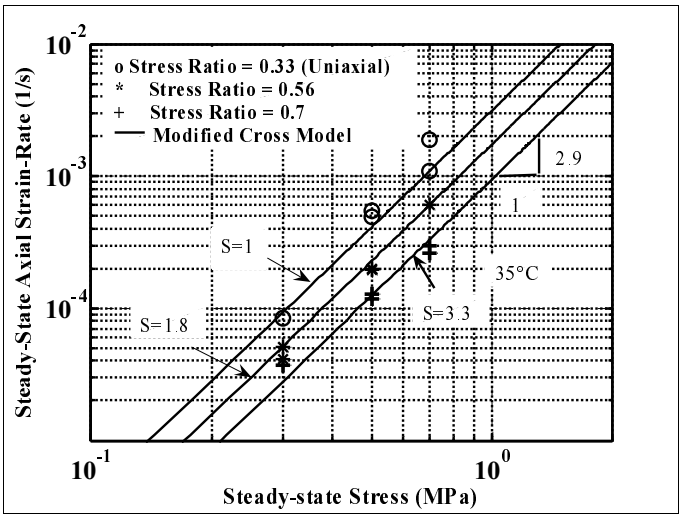


Fig. 14. Monotonic steady-state behaviour of the HRA at different stress ratios

The Modified Cross Model with the addition of a stiffening factor (as suggested by Deshpande *et al.* [8]) is given by:

$$\frac{\sigma}{\sigma_0} = \frac{\dot{\varepsilon}}{S\dot{\varepsilon}}\left\{1 + \left(\frac{\dot{\varepsilon}}{S\dot{\varepsilon}_p}\right)^m\right\}^{-1} \tag{7}$$

where $S$ is the stiffening factor. The value of $S$ was determined by fitting Eq. (7) to the experimental data using the constants in Table 4. The result is shown in Fig. 14 by the solid lines. It can be seen from Fig. 14 that, over the range of stress levels used in this study, the mixtures exhibit non-linear power law creep behaviour with the power exponent of 2.9. From Fig. 14 it can be seen that $S$ increases with increasing the stress ratio $\eta$. Figure 15 summarises the effect of the stress ratio on $S$ for the two mixtures. It can be seen from this figure that the stiffening factor is more sensitive to the stress ratio for the DBM compared to the HRA mixture. This was expected as the confinement has more effect where there is greater aggregate interlock, which is the case for the continuously graded DBM.

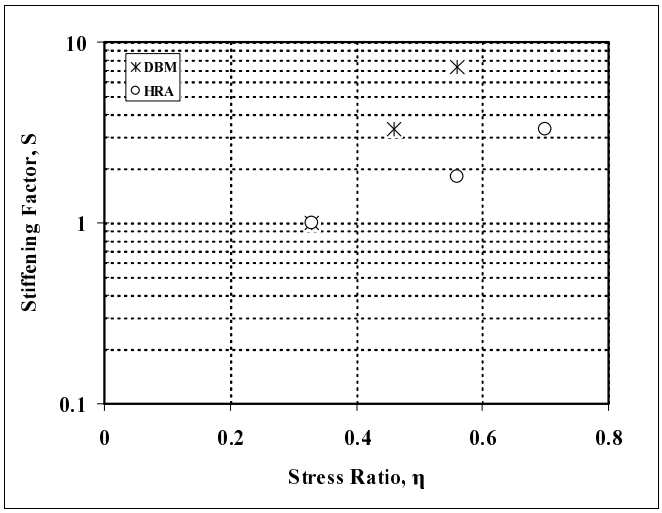


Fig. 15. Stiffening factor of the mixtures

## 5. CONCLUSION

The following conclusions can be drawn from this paper:

- Constant stress creep tests performed on the 70/100 Pen bitumen indicated that the deformation behaviour of the pure bitumen can be characterised by power law creep with the creep exponent of 1 at low stress levels (<100kPa), indicating linear behaviour, and the creep exponent of approximately 2.6 at high stress levels (>500 kPa), indicating non-linear viscous behaviour. The transition from linear to nonlinear behaviour was found to occur at a stress level of 11 kPa.
- The uniaxial and triaxial steady-state deformation behaviour of the HRA and the DBM mixtures was found to be linear viscous at low stress levels and non-linear viscous with an exponent of 2.9 for the HRA and 4 for the DBM mixture at high stress levels. The behaviour was found to be well captured by the Modified Cross Model.
- The temperature dependence of the uniaxial steady-state deformation behaviour was found to be well captured by WLF equation.
- Confinement was found to have a stiffening effect on the steady-state deformation behaviour with a greater effect for the mixture with the higher aggregate interlock.
- A critical stress ratio was found for each mixture, beyond which the mixtures were observed to lock-up.

## REFERENCES

1. Arabani, M. & Veis Karami, M. (2007). A simple nonlinear-elastic model for prediction of lime stabilized clayey sand behaviour. *Iranian Journal of Science and Technology Transaction B: Engineering,* Vol. 31, pp.573-576.
2. Collop, A. C., Cebon, D. & Hardy, M. S. (1995). Viscoelastic approach to rutting in flexible pavements. *Transportation Engineering,* Vol. 121, pp. 88-29.
3. Eisenmann, J. & Hilmer, A. (1987). Influence of wheel load and inflation pressure at asphalt pavements - experiments and theoretical investigations. *Proceedings of the 6th Inernational Conference on the Structural Design of Asphalt Pavements*, Ann Arbor, pp. 392-403.
4. Hofstra, A. & Klomp, A. J. G. (1996). Permanent deformation of flexible pavements under simulated road traffic conditions. *Proceedings of the Third International Conference on the Structural Design of Asphalt Pavements*, London, UK, pp. 613-621.
5. Cheung, C. Y. & Cebon, D. (1997). Deformation mechanisms of pure bitumen. *Materials in Civil Engineering*, Vol. 9, pp.117-129.
6. Cheung, C. Y. & Cebon, D. (1997). Experimental study of pure bitumen in tension, compression and shear. *Rheology*, Vol. 41, pp. 45-73.
7. Collop, A. C., Airey, G. D. & Khanzada, S. (2002). Creep testing of bitumens using the dynamic shear Rheometer. *Pavement Engineering* Vol. 3, pp.107-116.
8. Deshpande, V. & Cebon, D. (1999). Steady-state constitutive relationship for idealised asphalt mixes. *Journal of Mechanics of Materials*, Vol. 31, No. 4, pp. 271-297.
9. Collop, A. C. & Khanzada, S. (2001). Permanent deformation in idealised "Sand Asphalt" bituminous mixtures. *The International Journal of Road Materials and Pavement Design*, Vol. 2, No. 1, pp. 7-28.
10. Ossa, E. A. (2004). *Deformation behaviour of bitumen and bituminous mixes.* Ph.D. Thesis, University of Cambridge, Cambridge, UK.
11. British Standards Institution (2003). Coated macadams for roads and other paved areas. BS 4987: Part1.
12. British Standards Institution (2003). *Hot rolled asphalt for roads and other paved areas*. BS 594: Part1, London.

13. Taherkhani, H. (2006). Experimental Characterisation of the Compressive Permanent Deformation Behaviour in Asphaltic Mixtures. Ph.D Thesis, University of Nottingham, UK.
14. British Standards Institution (1989). *Sampling and examination of bituminous mixtures for roads and other paved areas*. Methods of test for the determination of density and compaction.
15. Airey, G. D. (1997). Rheological characteristics of polymer modified and aged bitumen. PhD Thesis, University of Nottingham.
16. Ossa, E. A., Deshpande, V. & Cebon, D. (2003). A phenomenological model for the monotonic and cyclic behaviour of pure bitumen. *Journal of Materials in Civil Engineering, ASCE*.
17. Deshpande, V. S. (1997). Steady-state deformation behaviour of bituminous mixes. Ph.D. Thesis, University of Cambridge, UK.
18. Cheung, C. Y. (1995). Mechanical behaviour of bitumens and bituminous mixes. Ph.D. Thesis, University of Cambridge, Cambridge.
19. Collop, A. C. & Khanzada, S. (1999). Permanent deformation behaviour of idealised bituminous mixtures. *Proc. 3rd European Symposium on Pperformance and Durability of Bituminous Materials and Hhydraulic Stabilised Composites*, Leeds UK, pp. 47-58.